Manganese-doped bismuth vanadate solid electrolytes

Part 1.—Synthesis and characterization of $Bi_2V_{1-x}Mn_xO_{5.5-x}$, $(0.1 \leqslant x \leqslant 0.25)$

Yuemei L. Yang, Longbao Qiu, William T. A. Harrison, Roy Christoffersen and Allan J. Jacobson*

Department of Chemistry, University of Houston, Houston, TX 77204-5641, USA

The solid solution series $Bi_2V_{1-x}Mn_xO_{5.5-x}$ $(0.10 \leqslant x \leqslant 0.25)$ has been prepared by conventional solid-state reaction and by crystallization from the melt. After additional subsolidus annealing both procedures yielded tetragonal phases with similar structures and lattice constants, as determined by X-ray powder diffraction. Partial substitution of manganese on the vanadium sites stabilizes $Bi_2V_{1-x}Mn_xO_{5.5-x}$ in the high-temperature tetragonal (γ) structure of $Bi_2VO_{5.5}$ for compositions in the range $0.10 \leqslant x \leqslant 0.25$. The structures of four compositions have been investigated by combined Rietveld refinements of X-ray and neutron powder diffraction data. Further characterization studies by transmission electron microscopy, magnetic susceptibility measurements and differential thermal analysis are described.

Very high oxide ion conductivity has been reported recently in a family of compounds derived from $Bi_2VO_{5.5}$ by partial substitution of vanadium with other metals.[1] The parent compound, $Bi_2VO_{5.5}$, is the first member $(n=1)$ of the Aurivillius family of structures with the ideal composition $Bi_2A_{n-1}B_nO_{3n+3}$.[2–8] The structure is comprised of $(Bi_2O_2)^{2+}$ sheets interleaved with $(VO_{3.5})^{2-}$ perovskite layers.[4–6] Oxygen vacancies located in the perovskite layer undergo ordering with decreasing temperature, leading to the formation of structurally distinct α, β and γ forms of the compound.[4] The structure of the lowest temperature phase, α, in which the vacancies are ordered, was determined recently and shown to contain V^{5+} ions in distorted tetrahedral and octahedral coordination by oxygen atoms.[9] On heating, the α phase transforms first to the intermediate β phase and then to the γ phase in which the oxygen vacancies are disordered.[4] The γ phase has a simple tetragonal structure with the ideal symmetry of the $n=1$ Aurivillius structure (*I*4/*mmm*). The unit cells of the α and β phases can be indexed with lattice constants corresponding to $6a\sqrt{2} \times a\sqrt{2} \times c$ and $2a\sqrt{2} \times a\sqrt{2} \times c$, respectively where a and c are the lattice constants of the tetragonal γ phase.[4,9,10] The ionic conductivity increases with each phase transition and is very high for the γ phase.[1]

Following the initial work on pure bismuth vanadate, many research groups have shown that the γ phase structure can be stabilized at lower temperature by partial substitution of vanadium with a large number of other metals.[1,11–22] Cation substitution suppresses vacancy ordering and leads to high ionic conductivity below the γ to β phase transition temperature. Substitution with Cu, Co and Ti results in unusually high ionic conductivity at lower temperatures.[1,11,14,15,21] The compositions of the substituted bismuth vanadates are usually written as $Bi_2V_{1-x}ME_xO_{5.5-y}$, where ME denotes a metal other than vanadium and y is dependent on the ME oxidation state. These oxides are often referred to as the BIMEVOX phases.

Because the BIMEVOX phases contain bismuth, they are susceptible to reduction at moderate oxygen partial pressures $(\lesssim 10^{-13}$ atm) and are therefore not suitable for applications as electrolytes in high-temperature fuel cells. They do however, have, potential applications in oxygen pumps, as electrode materials and as membranes for oxygen separation. The latter applications require, in addition to the high ionic conductivity, some significant electronic contribution to the total conductivity. For this reason, we have investigated dopant systems that could enhance the electronic conductivity. In the present work, we report our recent results on the synthesis and characterization of the compounds $Bi_2V_{1-x}Mn_xO_{5.5-x}$ for $0.10 \leqslant x \leqslant 0.25$. We have synthesized single-phase compositions in this range and characterized them with an emphasis on combined Rietveld refinements of X-ray and neutron powder diffraction data. Other techniques used are transmission electron microscopy (TEM), magnetic susceptibility and differential thermal analysis. The present paper is the first of a series of papers on the manganese-doped bismuth vanadate phases. In future papers, we will report measurements of ionic conductivity, oxygen permeation through membranes and an EXAFS study of the local structure.

Experimental

A series of single-phase polycrystalline samples of $Bi_2V_{1-x}Mn_xO_{5.5-x}$ $(0.10 \leqslant x \leqslant 0.25)$ were prepared from stoichiometric mixtures of pre-dried V_2O_5 (Aldrich, 99.6%), MnO_2 (Aldrich, 99%+) and Bi_2O_3 (Aldrich, 99.9%+). The mixtures were ground in an agate mortar and processed into the final powders by two principal methods that we call conventional annealing (CA) and melt crystallization and annealing (MA). A third method, melt crystallization and annealing followed by quenching (MAQ), was utilized as a method of obtaining quenched samples using material made initially by the MA procedure. All heating was carried out in air using Pt crucibles as containers.

In the CA procedure, the oxide mixtures were all processed in the temperature sequence: 500 °C for 4 h, 750 °C for 12 h, 850 °C for 20 h and 880 °C for 36 h, with regrinding after each step. The intermediate regrindings were very important for the formation of homogeneous single-phase samples. The samples then received a final 52 h heat treatment at slightly different temperatures depending on their compositions as follows: $x=0.1$, 875 °C; $x=0.15$, 878 °C; $x=0.20$, 885 °C; $x=0.25$, 890 °C. The samples were cooled from these temperatures in the furnace over a period of 16 h. The resulting polycrystalline samples had grain sizes of 50–100 μm and were shown to be single phases by X-ray powder diffraction.

The MA procedure also used a sequential set of heat treatments for initial processing of the starting mixtures, as follows: 500 °C for 4 h, 750 °C for 12 h and 850 °C for 20 h, with intermediate regrinding. The samples were then melted at 920 °C followed by rapid cooling to room temperature to induce crystallization. The resulting polycrystalline samples had grains 100–300 μm in diameter and were single phase, as indicated by X-ray powder diffraction. These melt-crystallized samples were then re-annealed for 32 h in the subsolidus at the same set of compositionally dependent temperatures used for the CA samples above, and similarly furnace cooled over 16 h. This final heat treatment did not produce any additional increase in the grain size of the samples and resulted in single-phase powders, as indicated by X-ray diffraction.

Because the end-stage heat treatment in both the CA and MA procedures involved a final cooling step that was fairly slow (16 h to reach room temperature), some of the $x=0.15$ product powder from the MA series was split into three samples that were re-heated at 850 °C, 600 °C and 450 °C respectively, and then quenched by transferring their Pt crucible to a cooled copper block. The resulting samples are designated MAQ1 (850 °C), MAQ2 (600 °C) and MAQ3 (450 °C).

Possible phase transitions and the melting behaviour of selected samples were studied using a Du Pont SDT2960 thermal analysis instrument. The instrument was calibrated against standard reference samples. Approximately 50 mg of the sample was used in each measurement. Data were recorded at $p(O_2)=0.21$ and 0.0015 atm (21% and 0.15% O_2 in Ar balance). Thermogravimetry data were collected simultaneously to determine any mass changes in the samples.

X-Ray powder diffraction data for the $Bi_2Mn_xV_{1-x}O_{5.5-x}$ sample series were collected on a Scintag XDS 2000 automated powder diffractometer [Cu-Kα radiation, $\lambda=1.541\,78$ Å and $T=25(2)$ °C, flat plate sample, θ–θ mode]. Initial measurements indicated strong preferred orientation effects. Samples were subsequently either ground thoroughly ($x=0.10, 0.15$) or ball-milled ($x=0.20, 0.25$) before the diffraction measurements. This resulted in similar patterns for all samples. All of the observed diffraction maxima could be indexed with tetragonal unit cells. For Rietveld analysis, X-ray data sets were collected in the range $10° < 2\theta < 90°$ with longer counting times (0.02° steps with a count time of 12 s per step).

Room-temperature high-resolution neutron powder diffraction data were collected for samples (*ca.* 10 g, vanadium cans) with $x=0.10$ and 0.15 on the HRNPD diffractometer at the High Flux Beam Reactor (HFBR) at Brookhaven National Laboratory. A data collection time of 12 h resulted in satisfactory counting statistics ($10° < 2\theta < 145°$; step size $=0.02°$; $\lambda=1.8857$ Å as precalibrated with Al_2O_3). Room-temperature data for samples with $x=0.20$ and 0.25 were collected using the 32-detector high-resolution diffractometer BT-1 at the National Institute of Standards and Technology (NIST), Gaithersburg. Samples (*ca.* 10 g) were sealed in vanadium cans and a neutron wavelength of 1.539 Å was selected as calibrated with alumina powder. Each data set was collected over a 12 h period (step size 0.05°) and collated using in-house software into one overall data set ($10° < 2\theta < 150°$) for analysis. Coherent neutron scattering lengths of $b(\mathrm{Bi})=0.853$, $b(\mathrm{Mn})=-0.373$, $b(\mathrm{V})=-0.038$, and $b(\mathrm{O})=0.581\times10^{-12}$ m were assumed.

Electron microprobe analysis was carried out on a JEOL SXA-8600 electron probe microanalyser (EPMA) for samples with compositions $x=0.15$ and 0.20 prepared by both CA and MA methods. Analytical standards were vanadium metal (V), bismuth germanate (Bi), Cu_2O (Cu) and $MnSiO_3$ (Mn). Raw analyses were corrected using $\phi(\rho z)$ procedures.[23]

Transmission electron microscope (TEM) observations of the samples, primarily for the purpose of studying their electron single-crystal diffraction patterns, were performed utilizing a JEOL 2000FX analytical TEM operating at 200 keV. Samples were prepared by suspending finely ground powders in high-purity acetone and transferring drops of the suspension to a holey carbon support film on a 200 mesh Cu grid. After being characterized by electron diffraction and bright-field imaging, grains on the support film were also chemically analysed using the microscope's Link EXL energy-dispersive X-ray spectrometer system. This was done primarily to correlate any grain-to-grain differences in relative Bi, Mn and V concentrations with any variations in the corresponding electron diffraction patterns. For this purpose the X-ray peak intensities were compared directly and full quantification of the spectra using K-factors[24] was not carried out.

Magnetic susceptibility data were obtained between 4.2 and 300 K in an applied field of 6 kG using a Quantum Design Model MPMS SQUID magnetometer.

Results and Discussion

X-Ray and electron diffraction

X-Ray powder diffraction data confirmed that samples of $Bi_2V_{1-x}Mn_xO_{5.5-x}$ prepared by all three synthesis procedures are single phase with tetragonal unit cells for the composition range $0.10 \leqslant x \leqslant 0.25$. For each composition the diffraction patterns of samples prepared by the different methods are identical in their line positions; however, the patterns for the MA samples have somewhat sharper peaks.

Microprobe analyses of $x=0.15$ and 0.20 samples prepared by the CA and MA methods show that, within experimental error, samples prepared with a given Mn content have the same composition for each preparation method. Samples also have their expected stoichiometries (within experimental error), however, the microprobe and analytical TEM measurements both show an 8–10% relative variation in composition between different analysed areas in the same sample.

The results of an electron diffraction study of two $x=0.15$ samples, one prepared by the MA method, and the other a re-heated and quenched split of this sample (MAQ1; 850 °C), are summarized in Fig. 1. For the MAQ1 sample, diffraction patterns show only main reflections consistent with the tetragonal, disordered γ structure [Fig. 1(a)]. Weak lines of diffuse intensity are, however, present between the $hk0$ reflections in c-axis diffraction patterns and more complex diffuse scattering is present in reciprocal lattice sections tilted a few degrees off the ***ab*** plane.

In contrast to the MAQ1 sample, patterns from the MA sample exhibit superlattice reflections as well as some different configurations of diffuse scattering [Fig. 1(b)–(d)]. Patterns with sharp superlattice reflections are of two principal types. The first and most common type, shown in Fig. 1(b), has bright superlattice reflections at $n/3$ positions along equivalent 110 rows, and weaker $n/3$ reflections along $\boldsymbol{a}^*$ and $\boldsymbol{b}^*$ [Fig. 1(b)]. Examination of multiple zones from grains with this type of pattern indicate that the corresponding superlattice has tetragonal symmetry with a $3a\times3a\times c$ periodicity, and reflections of the class $hk0$ are absent for $h+k=2n+1$. The pattern shows similarities to those reported by Abraham *et al.*[1]

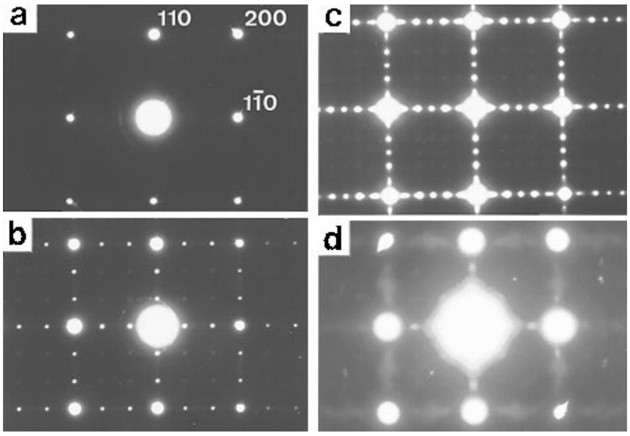

Fig. 1 Selected-area electron diffraction patterns for [001] zone axes in $Bi_2V_{0.85}Mn_{0.15}O_{5.35}$ samples. Indexing is based on the tetragonal unit cell for the disordered γ structure. (a) MAQ1 sample prepared with final quench from 850 °C. (b)–(d) Patterns from different grains in the same TEM sample of powder processed by the MA method.

and Pernot *et al.*[25] in slowly cooled samples of the Cu-doped BIMEVOX compounds $Bi_2V_{0.9}Cu_{0.1}O_{5.35}$ and $Bi_2V_{0.88}Cu_{0.12}O_{5.32}$, respectively.

The second type of pattern [Fig. 1(c)] has commensurate superlattice reflections at $n/2$ positions along $\boldsymbol{a}^*$ and $\boldsymbol{b}^*$ as well as incommensurate satellites along these rows. In these patterns strong intensity differences between the $\boldsymbol{a}^*$ and $\boldsymbol{b}^*$ rows, including complete extinction of one row relative to the other, are evident when the pattern is obtained with a small selected-area aperture. This suggests that the pattern may be averaging the scattering from multiple small domains with the orthorhombic α or β types of structure. A third type of pattern, shown in Fig. 1(d), does not exhibit sharp superlattice reflections but has arcs of diffuse intensity between the main reflections. It suggests that ordering of O vacancies and any other structural elements in the structure is of a short-range type, whereas the other two pattern types are consistent with longer-range correlations in the vacancy distribution. Although patterns of the first type dominate in the MA sample, the presence of all three pattern types indicates measurable variability in how structural ordering has proceeded as the sample cooled. This variation is most probably linked to the local variations in the cation stoichiometry, particularly the Mn content, that are indicated by the microprobe and analytical TEM results.

Thermal analysis and magnetic properties

The differential thermal analysis (DTA) data for $Bi_2V_{1-x}Mn_xO_{5.5-x}$ $(0.10 \leqslant x \leqslant 0.25)$ samples (both CA and MA) show no evidence for $\alpha \rightarrow \beta$ or $\beta \rightarrow \gamma$ phase transitions below the melting temperature. These data are consistent with the X-ray results and indicate that the high-temperature γ phase is stabilized by the partial substitution of manganese for vanadium atoms. A representative DTA scan for the composition $x = 0.15$ (A) collected at $p(O_2) = 0.21$ atm is shown in Fig. 2. A single transition is observed on heating at 910 °C, corresponding to sample melting. On cooling the reverse transition occurs at 872 °C. The transition temperatures measured for other compositions were essentially the same, within experimental error, and show little dependence on composition. Transition temperatures are unchanged (±2 °C) on lowering the oxygen partial pressure to $p(O_2) = 1.5 \times 10^{-3}$ atm. To our knowledge, the phase diagram of manganese-doped bismuth vanadates has not been determined. The phase diagram of the germanium-doped bismuth vanadate system, however, also shows only a weak dependence of the melting temperature on the concentration of the germanium dopant.[18]

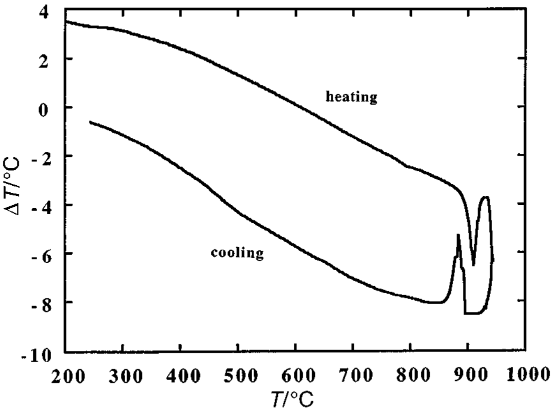

Fig. 2 DTA data for $Bi_2V_{0.85}Mn_{0.15}O_{5.35}$ (CA)

Thermogravimetric measurements were carried out during the DTA scans. The mass changes are small because of the large molecular mass and are difficult to measure with precision. The mass changes observed below 800 °C at $p(O_2) = 0.21$ atm corresponded to $\Delta y \leqslant 0.01$ in $Bi_2V_{1-x}Mn_xO_{5.5-x-\Delta y}$. Above 800 °C the mass changes were larger $(\Delta y \leqslant 0.06)$ and increased when the oxygen partial pressure was lowered to 1.5×10^{-3} atm $(\Delta y \leqslant 0.08)$. The mass changes are generally consistent with the magnetic susceptibility data described below.

Magnetic susceptibility data for the four different compositions are shown in Fig. 3. All of the data follow a Curie–Weiss law with the exception of the sample with $x = 0.25$ which shows evidence of a transition below 50 K. The data were modelled using $\chi = \chi_0 + C/(T - \theta)$, where χ is the measured magnetic susceptibility, χ_0 is a temperature-independent diamagnetic correction, C is the Curie constant, T the temperature (in K) and θ the Weiss constant. The results of the data fitting are given in Table 1. A comparison of the magnitudes of the observed magnetic moments with calculated values [calculated spin-only moments for high-spin octahedral complexes containing Mn^{4+} $(^4A_{2g})$, Mn^{3+} (^5E_g), Mn^{2+} $(^6A_{1g})$ are 3.87, 4.90 and 5.92 μ_B, respectively] indicates that the manganese ions are present predominantly as Mn^{3+} ions. The MnO_2 reactant used in the syntheses is apparently reduced during reaction.

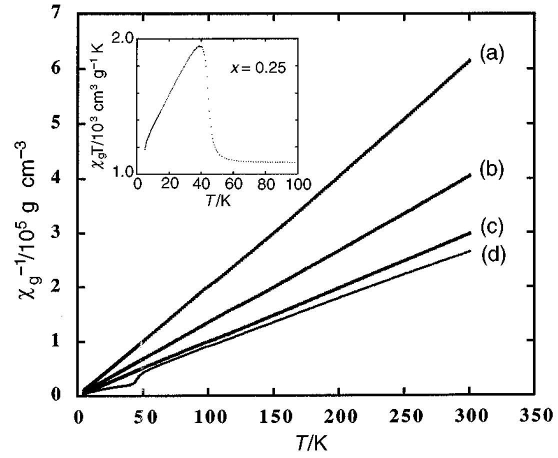

Fig. 3 Reciprocal magnetic susceptibility *vs.* temperature for $Bi_2Mn_xV_{1-x}O_{5.5-x}$ [$x = 0.10$ (a), 0.15 (b), 0.20 (c), 0.25 (d)] (MA). Inset shows χT *vs.* T for $Bi_2V_{0.75}Mn_{0.25}O_{5.25}$ in the vicinity of the transition.

Table 1 Magnetic susceptibility data for $Bi_2V_{1-x}Mn_xO_{5.5-x}$ samples

x	formula	M_r[b]	$C_g/cm^3\ g^{-1}$	θ/K	$C_M/cm^3\ mol^{-1}$	μ_{eff}/μ_B
0.10	$Bi_2V_{0.90}Mn_{0.10}O_{5.40}$	555.70	5.501×10^{-4}	−8	3.057	4.94
0.15	$Bi_2V_{0.85}Mn_{0.15}O_{5.35}$	555.10	7.839×10^{-4}	−2	2.908	4.82
0.15(MAQ3)[a]	$Bi_2V_{0.85}Mn_{0.15}O_{5.35}$	555.10	7.736×10^{-4}	−5	2.863	4.79
0.15(MAQ2)[a]	$Bi_2V_{0.85}Mn_{0.15}O_{5.35}$	555.10	8.622×10^{-4}	−5	3.191	5.05
0.15(MAQ1)[a]	$Bi_2V_{0.85}Mn_{0.15}O_{5.35}$	555.10	8.851×10^{-4}	−5	3.275	5.12
0.20	$Bi_2V_{0.80}Mn_{0.20}O_{5.30}$	554.50	1.144×10^{-3}	−12	3.171	5.04
0.25	$Bi_2V_{0.75}Mn_{0.25}O_{5.25}$	553.90	1.145×10^{-3}	−5	2.537	4.50

[a] MAQ3, MAQ2, MAQ1 refer to $x = 0.15$ samples quenched from 450 °C, 600 °C and 850 °C, respectively. [b] Molecular masses are calculated assuming V^V and Mn^{III}.

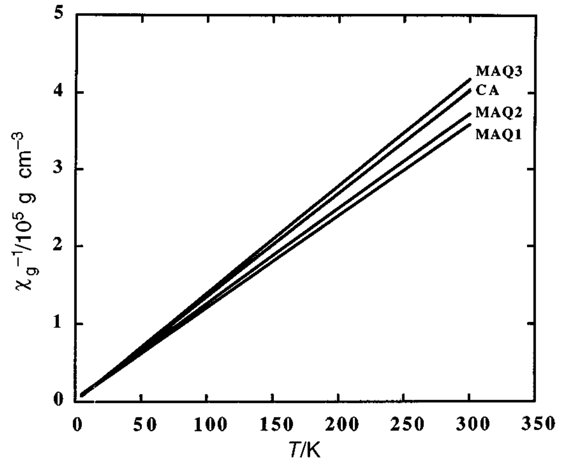

Fig. 4 Reciprocal magnetic susceptibility *vs.* temperature for $Bi_2V_{0.85}Mn_{0.15}O_{5.35}$ samples

Additional measurements were made on the three $x=0.15$ quenched samples MAQ1 (850 °C), MAQ2 (600 °C) and MAQ3 (450 °C). The results are shown in Fig. 4 together with data for a CA sample of the same composition that was furnace-cooled from 878 °C. All the data obey the Curie–Weiss law and the parameters obtained by fitting the data are also given in Table 1. The MAQ samples show small systematic changes in the magnitudes of their susceptibilities which correspond to an increase in the effective moment with increasing quench temperature. The effective magnetic moment of the MAQ1 sample is similar to that of the CA sample. The data for the quenched samples are consistent with the observed mass changes if it is assumed that some Mn^{3+} is reduced to Mn^{2+} at the higher quench temperatures.

A magnetic transition is observed for the sample with $x=0.25$ and is shown as an insert in Fig. 3 in the form a χT *vs.* T plot. The origin of this transition is not yet understood and will be the subject of further study.

X-Ray and neutron structure refinements

The X-ray powder diffraction data are dominated by scattering from the metal atoms in the structure, particularly from bismuth, whereas the neutron diffraction data are more sensitive to the positions and occupancies of the oxygen atoms and insensitive to the vanadium atoms. Consequently, joint Rietveld refinements of the X-ray and neutron diffraction data provide better overall sensitivity to the structural parameters and this analysis approach was used to investigate each of the four compositions. The program package GSAS was used to analyse the data at each composition.[26]

The space group *I*4/*mmm* (no. 122)[27] was assumed based on previous work.[1] For the $x=0.20$ and 0.25 compositions, the starting atom positions used in the refinements were taken from the structural model for γ phases proposed by Joubert and co-workers.[22,28] In this model, Mn and V atoms are statistically distributed over the same site (8i) and the Bi_2O_2 layers are undistorted. The disorder in the structure is represented by locating V,Mn atoms and the apical [O(3)] and equatorial [O(2)] oxygen atoms of idealized $(V,Mn)O_6$ octahedra in higher multiplicity sites with fractional occupancies. The oxygen vacancies are confined to the O(2) and O(3) sites. The starting atom positions used in the refinements of the data for the $x=0.10$ and 0.15 compositions were similar except that the V,Mn atoms were fixed at the high-symmetry 2a position. Attempts to displace the V,Mn atoms from this position led to unstable refinements.

Table 2 Atomic positional/thermal parameters for $Bi_2V_{0.90}Mn_{0.10}O_{5.4}$

atom	W[a]	*x*	*y*	*z*	occupancy	*B*/Å^2
Bi(1)	4e	0	0	0.33142(7)	1	1.07(2)
V(1)	2a	0	0	0	0.90	1.31(15)[b]
Mn(1)	2a	0	0	0	0.10	1.31(15)[b]
O(1)	4d	0	1/2	1/4	1	0.82(2)
O(2)	16n	0	0.5435(24)	0.5265(3)	0.201	2.94(6)[b]
O(3)	16n	0	0.1218(11)	0.1001(2)	0.224	2.94(6)[b]

Profile *R* factors: neutron $R_p=12.2\%$, $R_{wp}=9.2\%$; X-ray $R_p=9.9\%$, $R_{wp}=7.9\%$. [a]Wyckoff letter. [b]Constrained equal.

Table 3 Atomic positional/thermal parameters for $Bi_2V_{0.85}Mn_{0.15}O_{5.35}$

atom	W[a]	*x*	*y*	*z*	occupancy	*B*/Å^2
Bi(1)	4e	0	0	0.33140(6)	1	1.06(1)
V(1)	2a	0	0	0	0.85	1.48(13)[b]
Mn(1)	2a	0	0	0	0.15	1.48(13)[b]
O(1)	4d	0	1/2	1/4	1	0.80(2)
O(2)	16n	0	0.5433(20)	0.5268(2)	0.197	2.88(5)[b]
O(3)	16n	0	0.1282(9)	0.0991(2)	0.221	2.88(5)[b]

Profile *R* factors: neutron $R_p=10.5\%$, $R_{wp}=7.8\%$; X-ray $R_p=9.6\%$, $R_{wp}=7.7\%$. [a]Wyckoff letter. [b]Constrained equal.

In all refinements, the V,Mn occupancies were fixed to the nominal values and isotropic thermal parameters were refined subject to the constraints that the values for V and Mn atoms and for O(2) and O(3) atoms were equal. The total occupancy for the O(2) and O(3) atoms was constrained to equal the composition calculated assuming that Mn and V are present as Mn^{3+} and V^{5+} respectively (see below). With these constraints, stable and satisfactory refinements were obtained for each composition. The refined atomic positions, thermal parameters and occupancies are given in Tables 2–5 for each composition. The lattice parameters and some selected bond distances are given in Table 6. The variation of the lattice constants with manganese concentration is shown in Fig. 5 and the profile fits for one composition ($x=0.2$) are shown in Fig. 6(a) and (b) for the neutron and X-ray diffraction data, respectively. The profile fits for the other compositions are available as supplementary material.[†]

The diffraction data for all samples were indexed using body-centred tetragonal unit cells with lattice constants given in Table 6. We note that the neutron diffraction data do contain weak, extra diffracted intensity, probably indicating some degree of oxygen vacancy ordering. The extra intensity is particularly noticeable in the range $30 \leqslant 2\theta \leqslant 45°$ [see Fig. 6(a)]. The variation of unit-cell constants with composition is shown in Fig. 5. The *c* axis increases at a decreasing rate with manganese substitution whereas the variation in the *a* axis length decreases for $x \leqslant 0.2$ and then increases between $x=0.20$ and 0.25. The variation of the *c* axis with composition for the manganese-containing samples is generally similar to results reported previously for other metal substituents (*e.g.* Cu,[14] Ni[12] and Co[15]). The reported variations in the *a* axes of other metal-substituted systems are small and apparently metal-specific.

The model proposed by Joubert[28] gives satisfactory fits to the X-ray and neutron diffraction data at all compositions. This model assumes an undistorted Bi_2O_2 layer with a Bi—O(1) distance of *ca.* 2.329 Å. The Bi—O distance varies little with the extent of manganese substitution. The distances to the apical oxygen atom, O(3), are in the range 2.65–2.68 Å with the slightly longer distance observed for the larger values of *x*. The Bi—O(2) (equatorial) distance is somewhat longer at 2.83–2.85 Å. In the Joubert model, the disorder in the structure is represented by partial occupancies for the O(2) and O(3) sites and displacements of these atoms from their

---

[†] Supplementary material (SUP No. 57190, 14 pages) has been deposited at the British Library. For details of the Supplementary Publications Scheme see Information for Authors, Issue 1.

Table 4 Atomic positional/thermal parameters for $Bi_2V_{0.80}Mn_{0.20}O_{5.30}$

atom	W[a]	x	y	z	occupancy	$B/Å^2$
Bi(1)	4e	0	0	0.33124(6)	1	0.83(1)
V(1)	8i	0.035(13)[b]	0	0	0.2	0.93(22)[b]
Mn(1)	8i	0.035(13)[b]	0	0	0.05	0.93(22)[b]
O(1)	4d	0	1/2	1/4	1	0.82(2)
O(2)	16n	0	0.5417(24)	0.5279(3)	0.197	2.39(5)[b]
O(3)	16n	0	0.1311(11)	0.1015(3)	0.216	2.39(5)[b]

Profile R factors: neutron $R_p=8.0\%$, $R_{wp}=6.5\%$; X-ray $R_p=10.0\%$, $R_{wp}=7.8\%$. [a]Wyckoff letter. [b]Constrained equal.

Table 5 Atomic positional/thermal parameters for $Bi_2V_{0.75}Mn_{0.25}O_{5.25}$

atom	W[a]	x	y	z	occupancy	$B/Å^2$
Bi(1)	4e	0	0	0.33133(7)	1	0.92(1)
V(1)	8i	0.047(11)[b]	0	0	0.1875	1.40(24)[b]
Mn(1)	8i	0.047(11)[b]	0	0	0.0625	1.40(24)[b]
O(1)	4d	0	1/2	1/4	1	0.95(2)
O(2)	16n	0	0.522(5)	0.5300(3)	0.192	2.62(6)[b]
O(3)	16n	0	0.1338(13)	0.1001(3)	0.214	2.62(6)[b]

Profile R factors: neutron $R_p=7.9\%$, $R_{wp}=6.3\%$; X-ray $R_p=10.2\%$, $R_{wp}=7.7\%$. [a]Wyckoff letter. [b]Constrained equal.

Table 6 Lattice constants and selected bond distances from the joint refinements of X-ray and neutron diffraction data for $Bi_2V_{1-x}Mn_xO_{5.5-x}$

	x			
	0.10	0.15	0.20	0.25
$a/Å$	3.92088(4)	3.91525(3)	3.91092(7)	3.91454(9)
$c/Å$	15.4382(2)	15.4895(1)	15.5158(3)	15.5253(7)
Bi—O(1)	2.3288(6)	2.3285(5)	2.3265(5)	2.3292(6)
Bi—O(2)	2.831(7)	2.832(6)	2.826(7)	2.853(14)
Bi—O(3)	2.676(3)	2.667(2)	2.645(3)	2.649(3)
V—O(2)	2.010(1)	2.008(1)	2.003(1)	2.030(6)
V—O(2)			2.15(5)	2.19(4)
V—O(2)			1.87(5)	1.84(4)
V—O(2)			2.026(8)	2.014(3)
V—O(2)av.	2.010	2.008	2.018	2.019
V—O(3)	1.618(4)	1.613(3)	1.662(6)	1.651(7)
V—O(3)			1.704(20)	1.708(18)
V—O(3)			1.618(12)	1.591(10)
V—O(3)av.	1.618	1.613	1.662	1.650

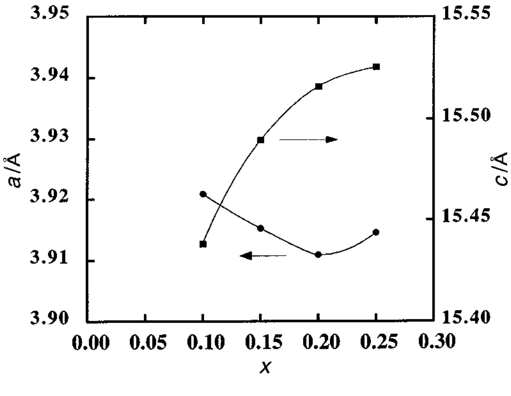

Fig. 5 Variation of the lattice parameters with x for $Bi_2V_{1-x}Mn_xO_{5.5-x}$

ideal positions. For the $x=0.2$ and 0.25 compositions additional disorder is represented by displacements of the V,Mn atom from the 2a site. This latter displacement results in a range of V—O distances as shown in Table 6. For comparison, the average apical and equatorial bond distances are also given in Table 6 and can be seen to vary little with composition. The model indicates the presence of vacant sites in both the apical and equatorial positions but with a larger fraction of the apical oxygen atoms vacant. The vacancy distribution is consistent with the presence of some V atoms in square-pyramidal coordination, but the presence of some vacancies in the equatorial site also suggests the presence of some tetrahedrally coordinated V atoms as observed in the structures of α-$Bi_2VO_{5.5}$[9] and $Bi_6V_3O_{16}$.[29]

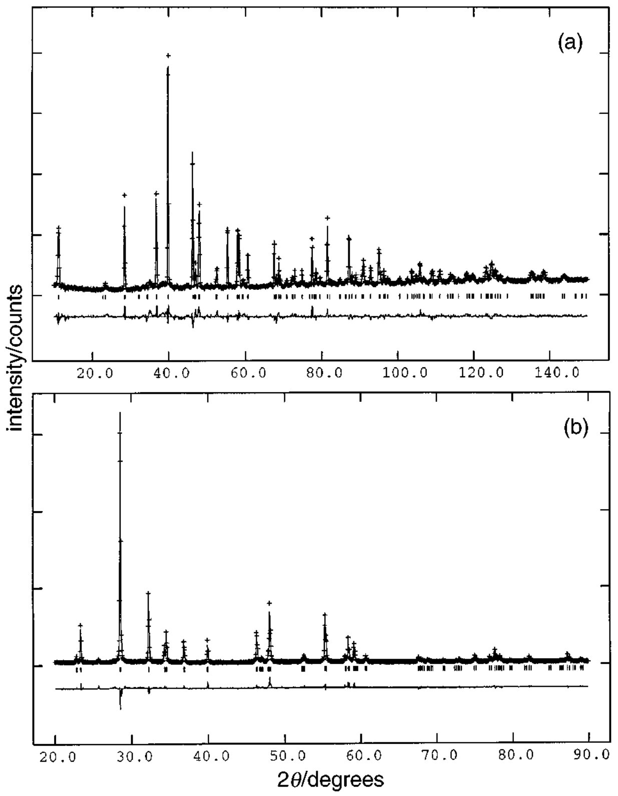

Fig. 6 Final observed (crosses), calculated (line) and difference profiles for the Rietveld refinement of (a) the neutron diffraction data and (b) the X-ray diffraction data for $Bi_2V_{0.80}Mn_{0.20}O_{5.30}$ Allowed reflection positions are indicated by tick marks.

Only limited information can be extracted from the bond distances derived for the average unit cell in a structure with substantial positional disorder. The values that are derived for the bond distances depend on the specific model that is chosen and more than one model may adequately represent the data. For example, in this particular case we have considered two additional models to represent the data at $x=0.2$. These two models were used previously to refine neutron diffraction data for BiNiVO$_x$ ($x=0.1$, 0.15, 0.20) model II,[12] and to refine single-crystal X-ray diffraction data for $BiCoVO_x$ ($x=0.10$) model III.[30] The major difference between these models and the one discussed earlier (model I) is that disorder is introduced into the Bi_2O_2 layers by placing Bi on a higher multiplicity site (model II) and by including in addition a second Bi site to effectively introduce disorder in the Bi position along *c*. The degree of disorder in the equatorial oxygen layer is reduced in both models II and III. Refinement of our data for $x=0.2$ using model II or III gives comparable *R* factors to refinements with model I. The details of these refinements and a comparison of the bond distances are available as supplementary material.

Conclusion

The tetragonal (γ) structure is obtained for manganese-doped bismuth vanadates $Bi_2Mn_xV_{1-x}O_{5.5-x}$ in the composition range $0.1 \leqslant x \leqslant 0.25$. No indication of $\alpha \rightarrow \beta$ or $\beta \rightarrow \gamma$ phase transitions are detected by DTA. However, electron diffraction patterns do show the formation of tetragonal ordered superstructures based on the γ structure in slowly cooled specimens. Magnetic susceptibility data indicate that manganese atoms are present as Mn^{3+} cations and that at temperatures above 650 °C further reduction to Mn^{2+} occurs. The X-ray diffraction and neutron diffraction data show that considerable structural disorder is present, as observed in other substituted bismuth vanadates and high-temperature γ-$Bi_2VO_{5.5}$. The results of joint refinements of the X-ray and neutron data are in general agreement with previous data and indicate that vanadium is present in more than one coordination environment. The detailed interpretation of the diffraction data in terms of bond distances and angles is dependent on the model used to describe the average unit cell contents.

We thank the Texas Center for Superconductivity, DOE through Los Alamos National Laboratory, and the Robert A. Welch Foundation for financial support of this work. We are grateful to J. Meen for the electron microprobe data and to D. P. Goshorn for the magnetic susceptibility data. We also express appreciation to J. Nicol at the National Institute of Standards and Technology and T. Vogt at Brookhaven National Laboratory for the neutron diffraction data.

References

1 F. Abraham, J. C. Boivin, G. Mairesse and G. Nowogrocki, *Solid State Ionics*, 1990, **40/41**, 934.

2 A. A. Bush and Y. N. Venevtsev, *Russ. J. Inorg. Chem.*, 1986, **31**, 769.

3 Y. N. Blinovskov and A. A. Fotiev, *Russ. J. Inorg. Chem.*, 1987, **32**, 145.

4 F. Abraham, M. F. Debreuille-Gresse, G. Mairesse and G. Nowogrocki, *Solid State Ionics*, 1988, **28/30**, 529.

5 M. Touboul and C. Vachon, *Thermochim. Acta*, 1988, **133**, 61.

6 K. B. R. Varma, G. N. Subbanna, T. N. Guru Row and C. N. R. Rao, *J. Mater. Res.*, 1990, **5**, 2718.

7 M. Touboul, J. Lokaj, L. Tessier, V. Kettman and V. Vrabel, *Acta Crystallogr., Sect. C*, 1992, **48**, 1176.

8 C. K. Lee, D. C. Sinclair and A. R. West, *Solid State Ionics*, 1993, **62**, 193.

9 O. Joubert, A. Jouanneaux and M. Ganne, *Mater. Res. Bull.*, 1994, **29**, 175.

10 R. N. Vannier, G. Mairesse, F. Abraham, G. Nowogrocki, E. Pernot, M. Anne, M. Bacmann, P. Strobel and J. Fouletier, *Solid State Ionics*, 1995, **78**, 183.

11 T. Iharada, A. Hammouche, J. Fouletier, M. Kleitz, J. C. Boivin and G. Mairesse, *Solid State Ionics*, 1991, **48**, 257.

12 M. Anne, M. Bacmann, E. Pernot, F. Abraham, G. Mairesse and P. Strobel, *Physica B*, 1991, **180/181**, 621.

13 R. N. Vannier, G. Mairesse, G. Nowogrocki, F. Abraham and J. C. Boivin, *Solid State Ionics*, 1994, **53/56**, 713.

14 J. B. Goodenough, A. Manthiram, M. Paranthaman and Y. S. Zhen, *Mater. Sci. Eng. B*, 1992, **12**, 357.

15 R. Essalim, B. Tanouti, J-P. Bonnet and J. M. Reau, *Mater. Lett.*, 1992, **13**, 382.

16 V. Sharma, A. Shukla and J. Gopalakrishnan, *Solid State Ionics*, 1992, **58**, 359.

17 R. N. Vannier, G. Mairesse, F. Abraham and G. Nowogrocki, *J. Solid State Chem.*, 1993, **103**, 441.

18 C. K. Lee, M. P. Tan and A. R. West, *J. Mater. Chem.*, 1994, **4**, 525.

19 R. N. Vannier, G. Mairesse, F. Abraham and G. Nowogrocki, *Solid State Ionics*, 1994, **70/71**, 248.

20 C. K. Lee, G. S. Lim and A. R. West, *J. Mater. Chem.*, 1994, **4**, 1441.

21 J. Yan and M. Greenblatt, *Solid State Ionics*, 1995, **81**, 225.

22 O. Joubert, M. Ganne, R. N. Vannier and G. Mairesse, *Solid State Ionics*, 1996, **83**, 199.

23 G. F. Bastin, F. J. J. van Loo and H. J. M. Heijliger, *Evaluation of the Use of Gaussian φ (ρz) Curves in Quantitative Electron Probe Microanalysis: A New Optimization*, University of Technology, Eindhoven, The Netherlands 1982.

24 G. Cliff and G. W. Lorimer, *J. Microsc.*, 1975, **103**, 203.

25 E. Pernot, M. Anne, M. Bacmann, P. Strobel, J. Fouletier, R. N. Vannier, G. Mairesse, F. Abraham and G. Nowogrocki, *Solid State Ionics*, 1994, **70/71**, 259.

26 A. C. Larson and R. B. von Dreele, *GSAS User Guide*, Los Alamos National Laboratory, New Mexico, 1990.

27 *International Tables for X-Ray Crystallography*, Kynoch Press, Birmingham, 1974, vol. IV, Table 2.3.1.

28 O. Joubert, Thesis, Nantes, 1992.

29 O. Joubert, A. Jouanneaux and M. Ganne, *Nucl. Instrum. Methods Phys. Res. B*, 1995, **97**, 119.

30 S. Lazure, R. Vannier, G. Nowogrocki, G. Mairesse, C. Muller, M. Anne and P. Strobel, *J. Mater. Chem.*, 1995, **5**, 1395.

Paper 6/04694K; *Received* 4*th July*, 1996